IEEE Access
Multidisciplinary | Rapid Review | Open Access Journal

Received March 19, 2021, accepted April 26, 2021, date of publication May 7, 2021, date of current version May 17, 2021.

Digital Object Identifier 10.1109/ACCESS.2021.3078252

Filtered Multicarrier Waveforms Classification: A Deep Learning-Based Approach

KAWTAR ZERHOUNI[1], EL MEHDI AMHOUD[1], (Member, IEEE), AND MARWA CHAFII[2], (Member, IEEE)

[1]School of Computer Science, Mohammed VI Polytechnic University, Ben Guerir 43150, Morocco
[2]Information Processing and System Teams (ETIS), CNRS, UMR 8051, École Nationale Supérieure de Électronique et de ses Applications (ENSEA), CY Cergy Paris Université, 95000 Cergy, France

Corresponding author: Kawtar Zerhouni (kawtar.zerhouni@um6p.ma)

ABSTRACT Automatic signal recognition (ASR) plays an important role in various applications such as dynamic spectrum access and cognitive radio, hence it will be a key enabler for beyond 5G communications. Recently, many research works have been exploring deep learning (DL) based ASR, where it has been shown that simple convolutional neural networks (CNN) can outperform expert features based techniques. However, such works have been primarily focusing on single-carrier signals. With the advent of spectrally efficient filtered multicarrier waveforms, we propose in this paper, to revisit the DL based ASR to account for the variety and complexity of these new transmission schemes. Specifically, we design two types of classification algorithms. The first one relies on the cyclostationarity characteristics of the investigated waveforms combined with a support vector machine (SVM) classifier; while the second one explores the use of a four-layer CNN which performs both features extraction and classification. The proposed approaches do not require any a priori knowledge of the received signal parameters, and their performance is evaluated in a multipath channel through simulations for a signal-to-noise ratio (SNR) ranging from -8 to 20 dB. The simulation results show that, despite cyclostationary characteristics being highly discriminative, the CNN outperforms the cyclostationary based classification especially for short time received signals, and low SNR levels.

INDEX TERMS Automatic signal recognition, multicarrier waveforms, classification, deep neural networks, support vector machines, cyclostationarity.

I. INTRODUCTION

Wireless communication has profoundly changed our societies, driving us forward from the industrial revolution to the networked era. It has transformed individuals from passive consumers to active content creators across many fields. Such technology has taken on a renewed significance since 2020, due to the COVID-19 pandemic [1]. Whereas social distancing policies were imposed, universities and businesses around the globe shifted to using digital solutions to fight this crisis and provide essential services such as virus spread monitoring, e-learning and online delivery services. However, all these crucial applications and many more heavily rely on reliable, high speed and secure communications, putting tremendous pressure on wireless systems.

Undeniably, this pandemic is validating the need of continuous connectivity, which could be achieved through flexible design of radio transceivers. In this context, multicarrier waveforms are great contenders to achieve such a flexibility, with orthogonal frequency division multiplexing (OFDM) being the most adopted one in current wireless systems. Its implementation is straightforward through inverse fast fourier transform (IFFT)-fast fourier transform (FFT), and its orthogonality both in time and frequency, allows a simple per-subcarrier one tap equalization. However, its strict synchronization needs, and low spectral containment, has led to the development of multiple candidate waveforms over the course of the last years. To relax the orthogonality condition, multicarrier waveforms rely on different design of synthesis functions. In this work, we focus on two families:

- *Per-subcarrier* filtered multicarriers: generalized frequency division multiplexing (GFDM) [2], and filter bank multicarrier (FBMC) [3], [4].
- *Per-subband* filtered group: universal filtered multicarrier (UFMC) [5], [6], and filtered orthogonal frequency division multiplexing (F-OFDM) [7], [8].

The associate editor coordinating the review of this manuscript and approving it for publication was Leandros Maglaras.

Performance comparison between the aforementioned waveforms has been a hotspot in recent years, as witnessed by the large publication record [9], [9]–[11]. Moreover, from the analysis of the waveforms frequency localization and spectral efficiency, it was established that each multicarrier waveform is suitable for a different application. Hence these waveforms are still considered as strong candidates for beyond 5G technologies [12]–[15].

Furthermore, the flexibility of transceivers can be achieved at the receiver side through automatic signal recognition (ASR). Traditionally, this function was mostly used with single-carrier signals and OFDM, and was adopted for both civilian and military applications to achieve automatic receiver configuration, interference mitigation, anti-jamming [16], spectrum monitoring, and primary user identification. Commonly, ASR has been subdivided into subcategories then studied separately [17]. These categories include, but are not limited to, automatic modulation classification (AMC) which aims at classifying the modulation scheme, and wireless technology recognition (WTR) which targets the more general task of identifying concurrent technologies. Either way, ASR has been dominantly achieved based on signal processing techniques, often times paired with machine learning (ML) classifiers [17]. These techniques comprise likelihood-based (LB) approaches, which considered optimal classifiers but at the expense of high computational complexity, and feature-based (FB) ones which are sub-optimal classifiers- widely investigated due to their lower complexity. For instance, the authors in [18] developed an algorithm to discriminate OFDM against single-carrier signals, using higher order cyclic cumulants (CC) under general conditions, including time dispersive channels and additive white Gaussian noise (AWGN). In [19], Spooner *et al.* designed a signal-processing system which blindly classifies, then estimates the parameters of several modulation schemes using the spectral correlation function (SCF) and higher-order CC paired to an unsupervised clustering algorithm for constellation-size estimation. Cyclostationarity based classifiers offer superior performance at very low signal-to-noise-ratio (SNR), but require high number of samples. A wavelet transform (WT) based higher-order statistical moments and a feed-forward artificial neural network (ANN) was adopted in [20] for modulation recognition. In [21], the authors proposed a classification method based on the fourth and sixth order cumulants paired with a support vector machine (SVM) classifier, performing good results at SNR $=$ 5 dB. In [22], a WTR algorithm was developed based on the received signal strength indicator (RSSI) to differentiate technologies such as Wi-Fi, long term evolution (LTE) and digital video broadcasting-terrestrial (DVB-T).

Driven by the complexity of feature extraction, especially given the diversity and heterogeneity of today's wireless technologies, a new paradigm based on deep learning (DL) techniques has been adopted in the last few years for ASR. In [23], O'Shea *et al*, introduced the novel idea of directly using the raw time domain in-phase and quadrature (I/Q) data combined with deep convolutional neural network (CNN) to avoid crafting expert features. The authors showed promising results for single-carrier modulation classification, outperforming traditional AMC methods. Following the same direction, while using the dataset called RML2016.10b [24], the authors in [16] proposed a CNN based AMC model, where a long symbol-rate observation sequence alongside an estimated SNR are used as training data, and a transfer learning method was introduced to improve the efficiency of retraining. In [25], the authors presented a generic methodology to easily design and implement DL based wireless signal classifiers, which was validated using the same RML2016.10b dataset. This leads to the conclusion that most of the new research efforts using DL techniques focus on single-carrier waveforms.

With the advent of the filtered multicarrier waveforms, it is of a prime importance to revisit DL-based ASR to account for the variety and complexity of these novel transmission mechanisms. Being relatively new waveforms, few works were reported in the direction of classifying the novel OFDM variants using DL models. To the best of the author's knowledge, the work in [26] was the first to apply neural networks for the classification of three of these new waveforms, namely UFMC, FBMC and OFDM. Based on a 7-layer CNN, the authors successfully classified the investigated signals, using amplitude data instead of I/Q, and improved the CNN performance through the use of principal component analysis (PCA). Therefore, the purpose of the present work is to extend the range of the investigated multicarrier waveforms, to account for the two main aforementioned filtered multicarrier families, while providing the following contributions:

- A novel cyclostationary features and SVM based waveforms classifier. Indeed, this is the first work that considers CC paired to ML techniques to classify the non-orthogonal multicarrier waveforms.
- A CNN based classifier, where the features are implicitly learned by the model from the I/Q input data.
- Both models are evaluated taking into consideration AWGN and multipaths fading channels.

The remainder of this paper is organized as follows. Section II introduces the signal models used herein. Section III details the proposed classification models. In Section IV the simulation environment is presented and results are discussed. Lastly, Section V concludes this work and sets future perspectives.

Notations: Δf stands for the subcarrier spacing, for a total number of subcarriers N_c. We consider critically-sampled discrete-time signal, where the sampling frequency is $f_s = \frac{1}{T_s} = N_c \Delta f$. The notation $(nT_s) \triangleq [n]$ is adopted, where n stands for time index. Time domain transmitted signals are denoted $x(\cdot)$, while $y(\cdot)$ represents their received counterparts. N is the multicarrier symbol spacing in time. $(.)_o$ subscript, denotes OFDM signal models. $(.)_g$ refers to GFDM signals, while $(.)_f$ is used for FBMC. UFMC signals are presented as $(.)_u$, finally $(.)_{fo}$ stands for F-OFDM. $\lceil(.)\rfloor$ indicates the

nearest integer function. $*$ is the linear convolution. Vectors are denoted by lowercase bold letters. $\tilde{(.)}$ is used to express the estimated value of (.).

II. SIGNAL MODEL

In a multicarrier transmission system, the transmitted signal can be represented by [9], [27]:

$$x[n] = \sum_{r=-\infty}^{\infty} \sum_{q=0}^{N_c-1} s_{q,r} g_{q,r}[n], \quad (1)$$

where $s_{q,r}$ denotes the transmitted data symbol on the q-th subcarrier during the r-th period. Without loss of generality, we consider the data symbols to be zero-mean independent and identically distributed (i.i.d) random variables, drawn from a quadrature amplitude modulation (QAM) constellation. $g_{q,r}[n]$ is the synthesis function which maps the data symbol to the waveform, and is given by:

$$g_{q,r}[n] = g_{tx}[\text{n-rN}]\, e^{j\frac{2\pi qn}{N_c}}, \quad (2)$$

with $g_{tx}[n]$ is the transmit prototype filter, which corresponds to a distribution of the symbol energy in frequency, time, or any other domain [9]. This definition of the synthesis function as given in (2) is also referred to as a *Gabor System* [9]. It implies that a single pulse shape is considered as a prototype and all others are shifted and modulated copies of this shape.

Considering propagation through a multipath channel, the signal is given by [27]:

$$r_{ch}[n] = x[n] * h[n] = \sum_{j=0}^{L_{ch}-1} h[\eta_j] e^{-j2\pi f_{d_j} n} x[n-\eta_j], \quad (3)$$

where η_j represents a discrete propagation delay. L_{ch} denotes the number of multipaths, and $h[\eta_j]$ is the time varying channel gain associated to the l-th path. $f_{d_j} = f_c \frac{v_d}{c}$ represents the motion induced-frequency shift, also known as the *Doppler shift*, where c is the speed of light and v_q is the relative speed between the transmitter and receiver.

Finally, we consider two impairments at the receiver: The symbol time offset δ, reflecting the unknown time of arrival of the signal, and the carrier frequency offset κ due to inaccuracy between transmitter and receiver oscillators. Hence the received signal can be expressed as:

$$y[n] = e^{j\frac{2\pi n\kappa}{N_c}} r_{ch}[n+\delta] + z[n], \quad (4)$$

where $z[n]$ is an additive Gaussian noise with variance σ_z^2.

It is well known from the Balian-low theorem (BLT) that there exists no prototype $g_{tx}[n]$ that achieves *orthogonality*, and which is well *localized* both in time and frequency, and achieves *critical density* [9], [28], [29]. Therefore, it has been common practice to deal with the limit of BLT by relaxing one of the three conditions.

Conventional OFDM is the special case where the frequency-localization has been relaxed. It is orthogonal, and achieves critical density. However its rectangular pulse shape, leads to a sinc-transfer function with very high out of band (OOB) emissions. In the presence of multipath channels, the multicarrier symbols overlap at the receiver introducing inter symbol interference (ISI). To address this problem, OFDM extends the symbol duration using a cyclic prefix (CP) of length $N_{cp} > \max(\eta_j)$. Hence, the received OFDM signal can be expressed as:

$$y_o[n] = e^{j\frac{2\pi n\kappa}{N_c}} \sum_{r=-\infty}^{\infty} \sum_{q=0}^{N_c-1} \sum_{j=0}^{L_{ch}-1} s_{q,r} h[\eta_j] e^{-j2\pi f_{d_j}(n+\delta)} e^{j\frac{2\pi q(n-\eta_j-rN_o+\delta)}{N_c}} + z[n], \quad (5)$$

where $N_o = N_c + N_{cp}$ is the OFDM symbol length.

A. UFMC AND F-OFDM SIGNALS

Motivated by the concept of resource block (RB) introduced in LTE system, UFMC subdivides the total bandwidth into N_c subcarriers, then groups them into S subbands, with Q subcarriers each [5], [30]. Each subband is filtered by a shifted version of the prototype filter $g[n]$, of length L. The centered filter is denoted by $g_Q[n] = g[n]\, e^{j\frac{2\pi Q/2n}{N_c}}$ [31]. Considering propagation through a multipath channel, the discrete-time baseband received UFMC signal can be expressed as follows:

$$y_u[n] = e^{j\frac{2\pi n\kappa}{N_c}} \sum_{s=0}^{S-1} \sum_{r=-\infty}^{+\infty} \sum_{q=0}^{Q-1} \sum_{j=0}^{L_{ch}-1} \sum_{l=0}^{L-1} s_{s,q,r} h[\eta_j] e^{-j2\pi f_{d_j}(n+\delta)} g_Q\left[n-l-\eta_j-rN_u+\delta\right] e^{j\frac{2\pi ql}{N_c}} e^{j\frac{2\pi(S_0+sQ)(n-\eta_j-rN_u+\delta)}{N_c}} + z[n], \quad (6)$$

where $s_{s,q,r}$ are the complex symbols transmitted on the q-th subcarrier in the s-th subband during the r-th period. S_0 stands for the starting frequency of the lowest subband. $e^{j\frac{2\pi(S_0+sQ)n}{N_c}}$ performs frequency shifting of both the data and filter coefficients to the appropriate subband.

A CP-variant of subband filtered technique namely F-OFDM, has also been proposed in [7], [32]. This waveform has the same signal model as UFMC but uses much longer filters of the order of half symbol duration to process the subband. It offers better spectral containment at the expense of ISI due to the filter tail. Both UFMC and F-OFDM are categorized as subband filtered multicarrier (SFMC) techniques.

B. FBMC SIGNAL

To address the lack of spectral containment of OFDM, FBMC focuses on improving the frequency localization using a prototype filter that spans over K multicarrier symbols in the time domain. The Martin-Bellanger-Mirabbasi [33]–[35] is such a filter that has been widely investigated in the recent years. It was adopted in the European project, Physical layer for dynamic access (PHYDYAS) [3], hence it is commonly referred to as the PHYDYAS filter. It offers very low OOB leakage at the expense of complex orthogonality. Indeed,

the chosen filter causes self-interference between subcarriers as well as between multicarrier symbols. To address this drawback, FBMC restores orthogonality in real-plane by mean of Offset Quadrature Amplitude Modulation (OQAM) operation. The QAM data symbols of the q-th subcarrier are converted to OQAM as explained in (7):

$$\text{for } q \text{ even } \begin{cases} u_{q,r'} = \Re(s_{q,r}) \\ u_{q,r'+1} = \Im(s_{q,r})j \end{cases}, \quad \text{for } q \text{ odd } \begin{cases} u_{q,r'} = \Im(s_{q,r})j \\ u_{q,r'} = \Re(s_{q,r}) \end{cases}, \tag{7}$$

where $\Re(s_{q,r})$ and $\Im(s_{q,r})$ represent the real and imaginary parts of $s_{q,r}$ respectively, and $r' = 2r$. The real and imaginary parts of the complex data symbol are transmitted with a half symbol time delay $\frac{N_c}{2}$. Defining $s^R_{q,r} = \Re(s_{q,r})$ and $s^I_{q,r} = \Im(s_{q,r})$, the received signal can be expressed as follows:

$$\begin{aligned} y_f[n] &= e^{j\frac{2\pi n\kappa}{N_c}} \sum_{r=-\infty}^{\infty} \sum_{q=0}^{N_c-1} \sum_{j=0}^{L_{ch}-1} j^q (-1)^r s^R_{q,r} h[\eta_j] \\ &\quad e^{-j2\pi f_{d_j}(n+\delta)} g\left[n - rN_c - \eta_j + \delta\right] e^{j2\pi q \frac{(n-rN_c-\eta_j+\delta)}{N_c}} \\ &\quad + e^{j\frac{2\pi n\kappa}{N_c}} j \sum_{r=-\infty}^{\infty} \sum_{q=0}^{N_c-1} \sum_{j=0}^{L_{ch}-1} j^q (-1)^r s^I_{q,r} h[\eta_j] e^{-j2\pi f_{d_j}(n+\delta)} \\ &\quad g\left[n - rN_c - \frac{N_c}{2} - \eta_j + \delta\right] e^{j2\pi q \frac{(n-rN_c-\frac{N_c}{2}-\eta_j+\delta)}{N_c}} + z[n]. \end{aligned} \tag{8}$$

C. GFDM SIGNAL

GFDM belongs to the same category as FBMC as it applies a per-subcarrier filtering. GFDM introduces the concept of *subsymbols* since each subcarrier caries, not only one, but M-QAM data symbols. To avoid the long filters of FBMC, GFDM applies circular pulse shaping of the individual subcarriers [2], which keeps the symbol's length unchanged before and after filtering. The received GFDM signal can be given by (9):

$$\begin{aligned} y_g[n] = e^{j\frac{2\pi n\kappa}{N_c}} &\sum_{r=-\infty}^{\infty} \sum_{q=0}^{N_c-1} \sum_{k=0}^{M-1} s_{q,k,r} \sum_{j=0}^{L_{ch}-1} \\ &h[\eta_j] e^{-j2\pi f_{d_j}(n+\delta)} g_D\left[n - kN_c - \eta_j - rN_g + \delta\right] \\ &e^{j\frac{2\pi q(n-\eta_j-rN_g+\delta)}{N_c}} + z[n], \end{aligned} \tag{9}$$

where $N_g = MN_c + N_{cp}$, and $s_{q,k,r}$ is the data symbol transmitted on the q-th subcarrier and k-th subsymbol during the r-th period [27]. The complex exponential applies the shifting of the prototype filter $g[n]$ in the frequency domain. $g_D[n] = g[n \bmod D]$ performs the circular shifting in time ($D = N_cM$) [36]. Mainly three filters are used for GFDM, the root raised cosine (RRC) filter, the raised cosine (RC) and the Xia filter.

The different filtering approaches adopted in the investigated waveforms, result in different power densities and spectral efficiencies [9]–[11], as well as different statistical features which can be used to classify these signals.

III. PROPOSED CLASSIFICATION MODELS

In this section, we present the different waveform classification models adopted in this paper. They fall in the scope of supervised learning, where the goal is to learn a mapping between input and output spaces, for a set of inputs $U = \{u_1, \ldots, u_m\}$ associated to a set of known outputs $V = \{v_1, \ldots, v_m\}$. Note that m stands for the number of available training examples. Generally speaking, in supervised learning, the available labeled data are split into a training set D and a testing set. Using the samples in the training set, the learning algorithm *infers a predictor* [37], which can then be used to predict the labels of newly acquired instances, such as the ones in the testing set. The latter are indeed used to evaluate the performance of the learned model.

Since the task of waveform identification aims at inferring discrete outputs, it can be treated as a multi-classification problem, where the input is the received complex discrete-time signals and the output is the transmitted waveform. Several ML algorithms can then be used to this end, such as the K-nearest neighbors (K-NN), decision trees, SVM and ANN. We focus on the last two ones as they have been extensively used for modulation recognition in single-carrier signals [19], [23], [38]–[40]. They both show comparable performance with the appropriate choice of their parameters. Most importantly, they can both learn non-linear functions -though with different approaches- which is relevant for multicarrier signals classification.

We extend the idea presented in [23] and explore the use of raw I/Q data for multicarrier waveforms with deep CNN, then compare it to a novel cyclostationary and SVM based classification routine as depicted in Fig. 1. Multicarrier signals are more complex compared to single-carriers, hence comparing the performance of implicitly learned features to hand crafted ones is interesting.

A. SUPPORT VECTOR MACHINES MODEL

SVMs classify the data by identifying the hyperplane which best separates one class from the others. The data instances closest to the hyperplane are called support vectors while their distance to the line is referred to as the margin [41]. The main goal of SVM then is to maximize this distance to ensure that the separation between classes is as wide as possible. SVM is different than ANN in that it does not suffer from the multilocal minima, hence it avoids overfitting [41]. Furthermore, it is a sparse technique; in fact, once the support vectors are identified, SVM relies only on this subset of the training data for future prediction. Kernels are adopted in practice to implement the SVM algorithm. They are used to transform the input space into higher dimensions, where the different classes can be linearly separable, thus reducing the complexity of the training. Common types of kernels include linear, polynomial and radial functions.

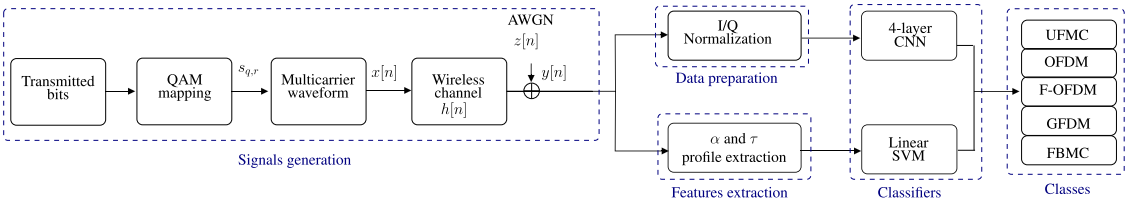

FIGURE 1. System model.

More formally, SVM aims at minimizing the objective function J such that [41]:

$$\begin{aligned} &\min_{\theta,\xi} J(\theta, b, \xi) = \frac{1}{2}\theta^T\theta + \lambda \sum_{i=1}^{m} \xi_i \\ &\text{subject to} \quad v_i(\theta^T \phi(u_i) + b) \geqslant 1 - \xi_i \\ &\qquad\qquad \text{and} \quad \xi_i \geqslant 0 \ \ \forall i, \end{aligned} \tag{10}$$

where θ is a weight vector, b is a bias, λ is a regularization term, and ξ_i are slack variables. $\phi(u)$ is a transform function, such that the kernel can be written as $K(u_i, u_j) = \phi(u_i).\phi(u_j)$. Note that (10) is the Soft-Margin primal form of the SVM, where slack variables are introduced to allow the model to misclassify few points when the data are not completely separable [41]. The learned parameters that solve this problem determine the final classifier $u_i \rightarrow \text{sign}(\theta^T \phi(u_i) - b)$, where sign(.) is the sign function.

Finally, SVM was initially introduced for binary classification problems; the simplest and most common way to extend it for multiclass problems is by implementing the *one versus rest* technique [41], where C binary SVMs will be trained independently to distinguish one class from all the others, C denoting the number of classes. In this paper, we use SVM in combination to manually extracted domain-specific features.

Proposed expert features vector:

One of the most distinctive features of communication signals is cyclostationarity. In fact modulated signals are often coupled with coding, pulse shaping, cyclic prefixes which leads to a built-in periodicity. Analysis of this property falls in the scope of cyclostationary signal processing, which has been extensively investigated in a wide variety of applications [42], [43]. A signal is wide sense cyclostationary of order m if its statistics of order m, are periodic functions of time. Such periodicity can be analyzed using Fourier series [27], [30], [43].

The cyclostationarity characteristics of multicarrier signals are relatively less explored compared to single-carrier ones. OFDM cyclostationarity is the one that has been widely studied and used for classification purposes. The m-th order cyclic cumulant of the subcarrier filtered family (GFDM and FBMC) has been recently reported in [27], while those of the subband filtered one (UFMC and F-OFDM) were published in [44]. In this paper, the 2^{nd} order, one conjugate cumulant, also known as the non-conjugate cyclic autocorrelation function (CAF) is used as it is sufficient to discriminate between the investigated waveforms [45]. Furthermore,

TABLE 1. Summary of cyclostationary properties of filtered multicarrier waveforms.

Waveform	Cyclic frequencies α [1]	Lags τ [1]
OFDM	rN_o^{-1}	$\pm N_c$
FBMC	$2rN_c^{-1}$	0
GFDM	$(M+\epsilon)N_g^{-1}$, $\epsilon = \lceil \frac{N_{cp}}{N_c} \rfloor$	0
	rN_g^{-1}	$a\ N_c, \ \mid \tau \mid \leq MN_c$
UFMC	rN_u^{-1}	$a\ \frac{N_c}{Q}, \mid \tau \mid \leq \frac{L}{2}$
F-OFDM	rN_{fo}^{-1}	$a\ \frac{N_c}{Q}$ and $\pm N_c$

[1] $r, a \in \mathbb{Z}$.

we define a reduced dimension version of CAF, separated into "α-profile" and "τ-profile" as depicted in Fig. 2 and Fig. 3. Note that the parameters used for these figures are the same ones reported in the simulation section in Table 3, for 100 symbols. As can be noticed, each waveform has a unique α and τ profile. First of all, for OFDM and the subband filtered family, the cyclic frequencys (CFs) are inversely proportional to the multicarrier symbol spacing, that is $\alpha = \frac{r}{N}$, $r \in \mathbb{Z}$ as shown in Fig. 2a, 2b. and 2c. OFDM exhibits cyclostationarity only at lag values proportional to the useful time of the multicarrier symbol, $\tau = N_c$, due to the use of CP, such behavior is depicted in Fig. 3a. Additionally, as one can notice in Fig. 3c, this property holds also for F-OFDM. Other signatures arise in lags proportional to $\frac{N_c}{Q}$ due to the subband filtering for UFMC and F-OFDM [44].

FBMC α-profile and τ-profile are presented in Fig. 2d and Fig. 3d respectively, its non-conjugate CAF exists only for lag $\tau = 0$, and CF proportional to the inverse of $\frac{N_c}{2}$. Finally, GFDM CFs are defined as $\frac{r}{N_g}$, at delay zero due to the circular filtering, and at delay $\tau = MN_c$ due to the CP insertion, where r is modeled as $r = (M + \epsilon)$, such that $\epsilon = \lceil \frac{N_{cp}}{N_c} \rfloor$ for $\tau = 0$, and $r \in \mathbb{Z}$ for the others [27]. A graphical representation of these properties is shown is Fig. 2e and Fig. 3e. Spectrum lines may however exist in some delays $\tau = \pm a\ N_c$, if the prototype filter is not ISI free [46], which is not the case for the RRC filter investigated in this paper. Finally, Table 1 summarizes the cyclostationary features of the investigated signals.

TABLE 2. Activation functions.

Name	g(z)	Range
ReLU	$max(0, z)$	$[0, \infty)$
SofMax	$\frac{e^{z_i}}{\sum_j e^{z_j}}$	$(0, 1)$

Since the CAF is mostly zero for non-CFs, we *blindly* construct a features vector comprising only of non-zero CAF values related to valid CFs and delays for each waveform. To this end, $\tilde{C}^{\alpha}_{2,1}(\tau)$, is first computed using the following consistent estimator [47]:

$$\tilde{C}^{\alpha}_{x}(\tau)_{(2,1)} = \frac{1}{N_s}\sum_{k=1}^{N_s} x[k]x^*[k+d]e^{-j2\pi\alpha k}, \tag{11}$$

where N_s denotes the total number of used samples. It is defined for a discrete CF domain $[-\frac{1}{2}, \frac{1}{2})$, where the resolution is $\Delta\alpha = \frac{1}{N_s}$.

We propose to perform lags estimation at CF zero. The magnitude of the CAF, $\tilde{C}^{0}_{2,1}(\tau)$ of the received discrete time signal is calculated over a range of positive delay values $V_\tau = [0 : \Delta\tau : d_{max}]$. In the current version of the proposed approach, the delay resolution $\Delta\tau$ and maximum d_{max}, are chosen to cover the possible peaks in the magnitude of the CAF, of the considered waveforms. The delay value $\tau_{candidate} \in V_\tau$, is tested using the cyclostationarity algorithm proposed in [47], applied to check whether $\alpha = 0$ is indeed a CF at this delay. If the test succeeded, $\tau_{candidate}$ is added to the delays vector $\tilde{\boldsymbol{\tau}}$. If no delay is recovered then the signal cannot be recognized.

Once $\tilde{\boldsymbol{\tau}}$ is defined, a vector of CFs is formed for each detected delay. Knowing that the CFs domain is symmetric, we limit the search set to its positive part $[0, \frac{1}{2})$. We use the conventional cyclostationarity test to check whether the estimated $\tilde{\alpha}$ is indeed a CF of the received signal at the investigated delay from $\tilde{\boldsymbol{\tau}}$. Let I be the estimation interval. The estimated CF, $\tilde{\alpha}$, can be expressed as [30], [48]:

$$\tilde{\alpha} = \arg\max_{\alpha\in I}(|\tilde{C}^{\alpha}_{2,1}(0)|^2). \tag{12}$$

Once a CF passes the test, it is removed, and the search is repeated until we construct a vector with n_c CFs for each delay.

B. CONVOLUTIONAL DEEP NEURAL NETWORKS MODEL

The core building block of any ANN is an artificial neuron, which is a simple computational unit that processes weighted inputs and produces an output using an activation function. Table 2 presents the activation functions used in this paper. A deep neural network (DNN) is an ANN with multiple hidden layers, $\boldsymbol{N}_L$, between the input layer and the output one.

In a traditional *flat* feedforward ANN, each hidden layer is made up of $\boldsymbol{n}_l$ neurons, each of which is fully connected to all neurons in the previous layer, while being independent from the ones in the same layer [49]. As its name suggests, this type of ANN requires the flattening of the training data into a 1-D vector. For images, the flattening of the pixels loses all of the spatial structure, and the full connectivity leads to a very high number of weights in larger images [50]. To circumvent these limitations, *convolutional* ANN re-arrange the neurons in 3 dimensions, then connect each neuron to only a local region of the input volume, hence preserving the spatial relationship between the input data while reducing the number of learnable parameters [49].

Communication signals are complex valued, thus, reshaping them from 1-D complex vectors, to 2-D I/Q vectors - to simulate an image- allows the use of the advances in CNN to extract features and perform the classification task directly from the raw received signals [24].

A CNN is made up of three types of layers, convolutional layer, pooling and fully connected [49]. The convolutional layer allows the extraction of a *filter map* from its input using filters, essentially the neurons of this layer. Pooling layers can be periodically inserted to reduce the spatial size of the representation and the number of parameters, hence allowing to control overfitting. This layer has no parameters to learn, and is used to compress or generalize feature representations. Finally, fully connected layers are used at the end of the network to create final nonlinear combinations of the learned features and to output probabilities of class predictions through the use of nonlinear activation functions. As the name implies, each neuron in this layer will be connected to all neurons in the previous one. Mathematically speaking, the convolutional layer can be represented by [16]:

$$u^l_i = g(\sum_{j=1}^{n_l-1} u^{l-1}_j * k^l_{i,j} + b^l_i), \tag{13}$$

where $l = 1 \ldots N_L$ is the layer index, $k^l_{i,j}$ are the convolution kernels or filter weights of the l-th layer and b is a bias. The *filter map* is in fact, the output of the kernels applied to the previous layer [50]. The pooling layer- which is optional and not adopted in the DNN architecture of the present work- reduces the dimensionality of its input vector according to the following equation [16]:

$$u^{l+1}_i = \text{down}(u^l_i), \tag{14}$$

where down(.) is a sub-sampling function computing maximum, average value, or L^2-norm of its input vector [40]. Finally, the fully connected layer, or dense layer, is described as:

$$U^l = g(\theta^l U^{l-1} + \boldsymbol{b}^l), \tag{15}$$

where $\boldsymbol{\theta}$ is the weight matrix and $\boldsymbol{b}$ is a bias vector. The convolutional and pooling layers can be viewed as the features extracting part of the DNN while the fully connected ones as the classifier. The overall DNN can be represented as follows:

$$V = G(U, \Theta), \tag{16}$$

where Θ are the entire network parameters and G is the overall learned function. Typically, a DNN does not learn perfect weights since there are too many unknowns. Instead,

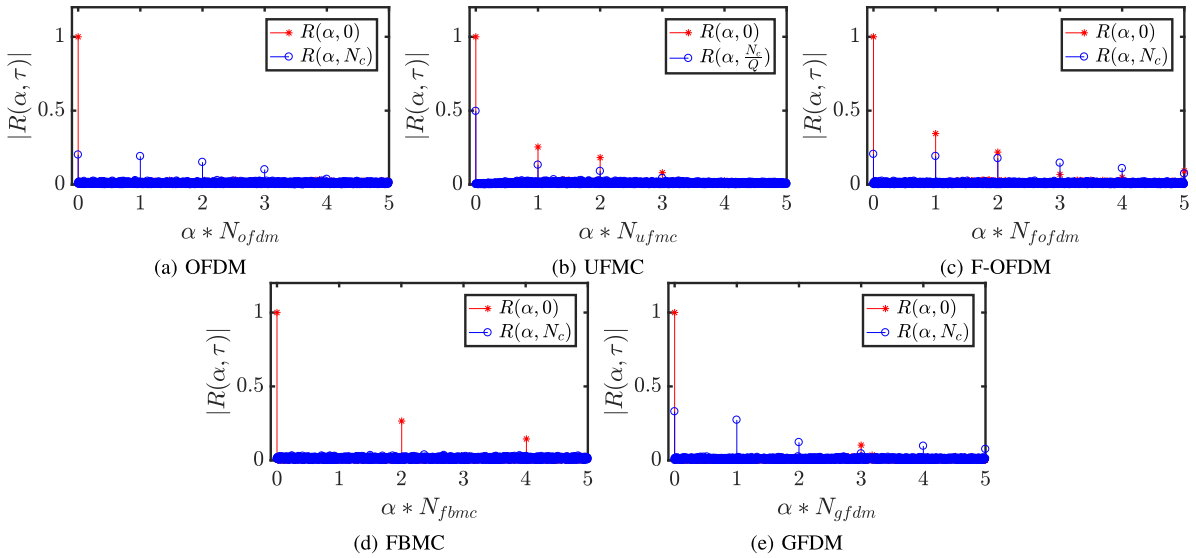

FIGURE 2. Cyclic frequency profile of the investigated waveforms.

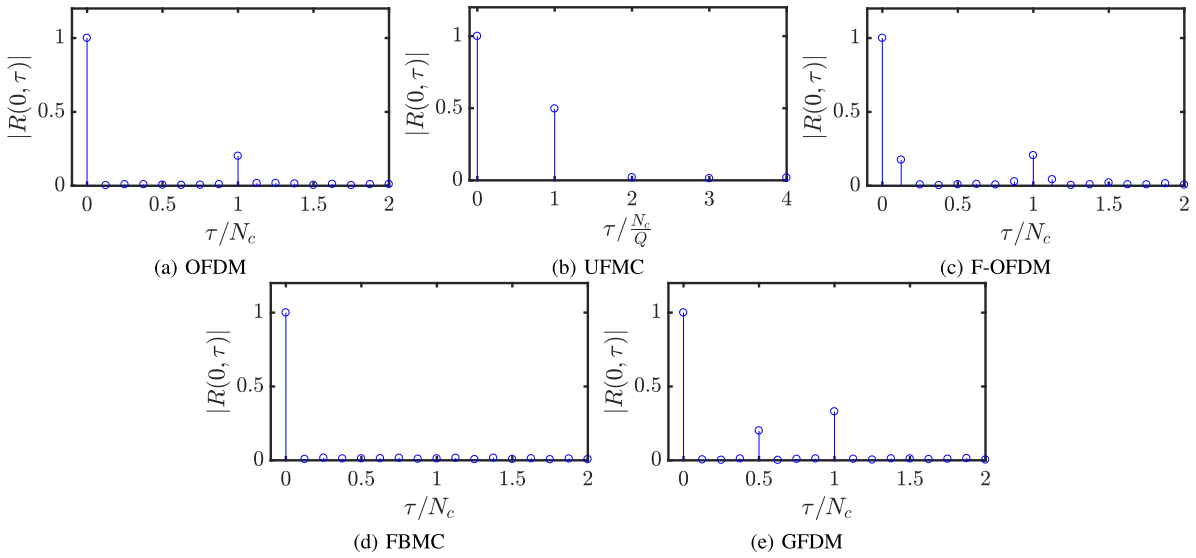

FIGURE 3. Lag profile of the investigated waveforms.

the problem of learning is seen as an optimization problem where an algorithm is used to navigate the space of possible sets of weights to minimize a loss function. To achieve this goal, DNN is typically trained using the popular stochastic gradient descent algorithm, which starts with some random initial weight values $\Theta = \Theta_0$ [40], then seeks to update them while reducing the gradient of the error, such that:

$$\Theta_{t+1} = \Theta_t + \eta \nabla J(\Theta_t), \tag{17}$$

where $\eta > 0$ denotes the learning rate, ∇ is the gradient operator, and $J(.)$ is the loss function (the objective function [51]). In this paper, we adopt the categorical cross-entropy [16], [40] loss function. In addition, the Adam optimization algorithm [52] is adopted instead of the classical stochastic gradient descent described in (17), where the learning rate η is not fixed, rather it is dynamically adapted to improve the convergence.

The convolutional DNN architecture of the network used in this paper is depicted in Fig. 4. It is inspired from the model used in [23], where the depth of the network is maintained to 4-layer in total, and divided in two convolutional layers and two dense fully connected ones, all using a ReLu activation function, except the last one where a SoftMax transfer function is adopted to output probabilities of class values directly. However, we change the number of filters, adopting 128 filters of length 1×3 in the first layer, followed by 80 filters of the same length in the second, while the dense layer is of length 128 neurons, then finally 5-classes neurons

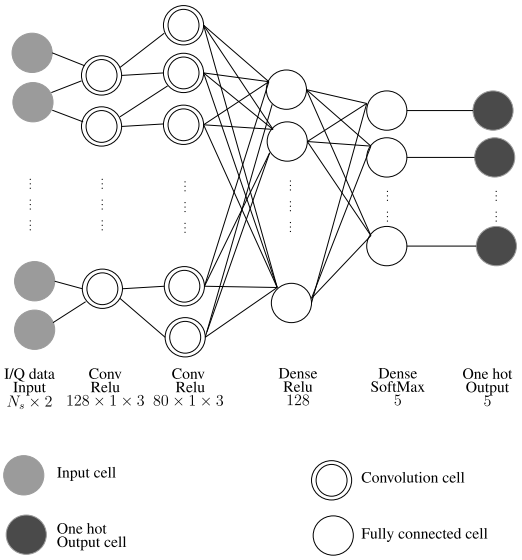

FIGURE 4. Deep neural networks architecture.

in the output one. After each one of the three first layers (2 Conv and one Dense) a dropout is used with a rate of $dr = 0.5$, to prevent overfitting. Learning is performed using the mini-batch gradient descent, where the training dataset is split into smaller *batches* used to calculate the model error and update its coefficients. This training procedure is repeated a number of times, referred to as *number of epochs*, until the total error of the model has been sufficiently minimized. In this paper, an early stopping method is used to stop training once the loss function of the model stops improving on a validation dataset, to avoid overfitting.

IV. METHODOLOGY, RESULTS, AND DISCUSSIONS

A. SIMULATION DETAILS

In this section, the performance of the proposed classification algorithms is analysed through numerical simulations. The investigated waveforms are generated using the parameters summarized in Table 3. We set the number of subcarriers to $N_c = 16$ for all the waveforms, except GFDM, for which $N_c = 8$, to generate signals with the same multicarrier symbol length. The cyclic prefix duration is set to $\frac{N_c}{4}$ which is larger than the maximum channel delay. We opt for the prototype filters proposed in literature, namely the Phydyas [3], [33], [35] for FBMC with an overlapping factor $K = 2$, the truncated sinc [7], [8] for F-OFDM where the filter length is set to $\frac{N_c}{2}$, the Chebyshev [5] for UFMC, and RRC for GFDM with a roll-off factor $\beta = 0.35$. The transmitted data symbols are from a quadrature phase shift keying (QPSK) constellation, and all signals have been normalized to have a unit power. We generate an overall database comprising of signals with $N_{symbols} = 100$, for an SNR ranging from -8 to 20 dB with an interval of 2 dB, with a number of examples equal to 5000 for each SNR. In order to simulate the impact of the multipath channel, we use the well known profile of the LTE channel model. More precisely, the extended typical urban

TABLE 3. Simulation parameters.

Parameter	Symbol	Value
Overall parameters		
Subcarrier spacing	Δf	15 kHz
Sampling time	T_s	$\frac{1}{\Delta f * N_c}$
IDFT size	N_c	16
CP length	N_{cp}	$N_c/4$
QAM	-	QPSK
UFMC		
Number of subbands	S	2
Subband size	Q	8
Filter type	-	Dolph-Chebyshev
Filter length	L_u	N_{cp}+1
Filter attenuation(dB)	-	40
F-OFDM		
Filter type	-	Truncated Sinc [8]
Filter length	L_{fo}	$N_c/2$
FBMC		
Filter type	-	Phydyas [3]
Overlapping factor	K	2
GFDM		
Number of subsymbols	M	2
Number of subcarriers	N_c	8
Filter type	-	RRC
Roll off	β	0.35

model (ETU) [53] is adopted. All signals are generated using Matlab, while the training is performed in Python, using Keras library with TensorFlow backend.

The confusion matrix is one of the most intuitive ways to visualise the results of a classification algorithm. In this research work, the simulation is performed for an SNR ranging from -8 to 20 dB, meaning that we have several confusion matrices to analyze. In this case other measures based on the confusion matrix can be used to assess the performance of the classification routines, such as the model's accuracy. A multi-class classification can be understood as a binary classification, where the class of interest c is *positive*, and all other classes are *negative*. A correct recognition for a class c is simply a *True Positive* (tp_c), while the correct recognition of all the other classes (c excluded) is a *True Negative* (tn_c). All other classes incorrectly declared as the class of interest c is a *False Positive* (fp_c), while the class c incorrectly predicted as any other class is a *False Negative* (fn_c). Using these four definitions, we can define the ***Average Accuracy*** as:

$$A = \frac{1}{C} \frac{\sum_{c=1}^{C} tp_c + tn_c}{tp_c + tn_c + fp_c + fn_c}. \tag{18}$$

It will be used to evaluate the overall effectiveness of the proposed classifiers, alongside the cross-entropy loss.

B. RESULTS AND DISCUSSIONS

In the 5G-New Radio (NR) configurations [54], the concept of subslot was introduced, where 2, 4 or 7 multicarrier

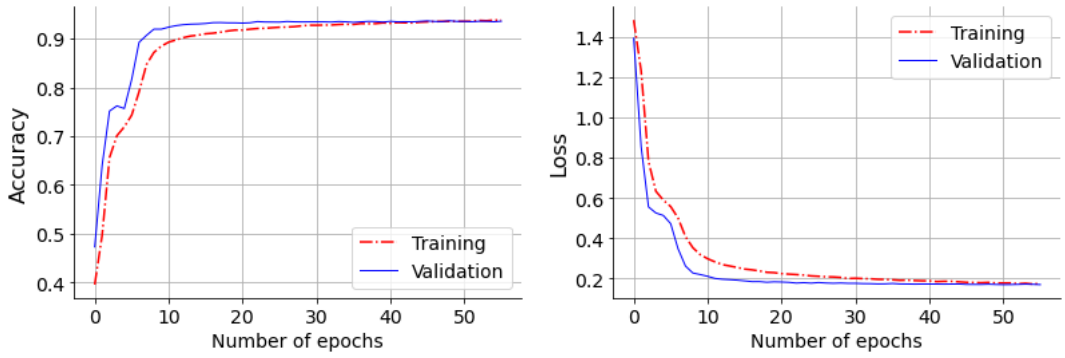

(a) accuracy (b) loss

FIGURE 5. Learning curves of the proposed CNN, with 128 samples.

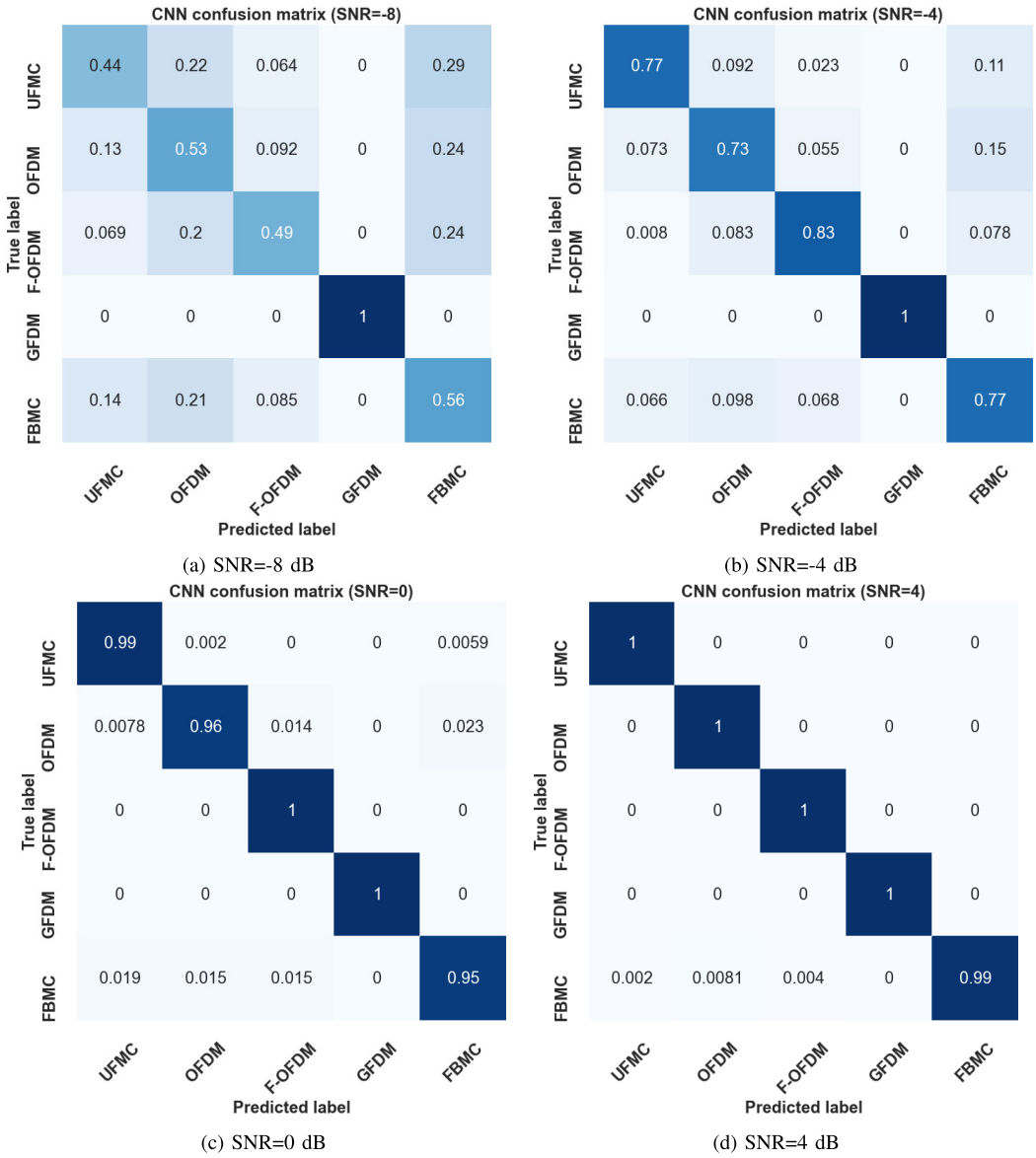

(a) SNR=-8 dB (b) SNR=-4 dB

(c) SNR=0 dB (d) SNR=4 dB

FIGURE 6. Confusion matrices of the proposed CNN, with 128 samples.

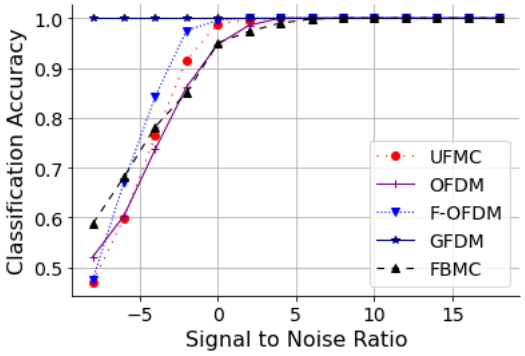

FIGURE 7. Per class accuracy for 128 samples.

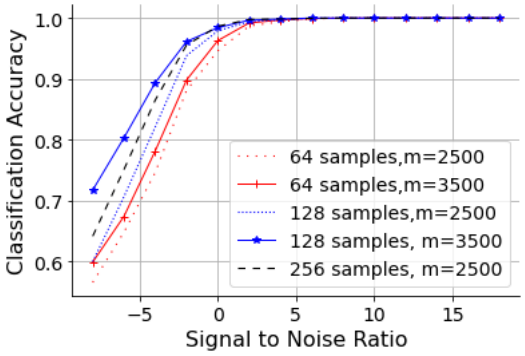

FIGURE 8. Accuracy comparison between 64, 128 and 256 samples.

symbols can be transmitted. We start by assessing the performance of the proposed algorithms using the smallest configuration, that is 2 multicarrier symbols. In our dataset, the smallest symbols are UFMC and OFDM with $N_u = N_o = 20$ samples each, while the longest is FBMC with $N_f = 40$ samples, whereas $N_g = 24$ and $N_{fo} = 28$. We evaluate the CNN architecture using $N_s = 64$ which captures at least 2 symbols of all the investigated waveforms except FBMC. Using half of the available examples (2500 examples per SNR), where 80% of the data is used for training and 20% for validation and testing, we reach a total accuracy of 0.92 across all SNR values, for roughly 7 minutes training. Notice that we use a vector of $N_s = 64$ for the I/Q data, per example, per waveform, per SNR. In a second configuration, we double the number of samples to capture multicarrier signals of length 128 (separated again into 128 I, and 128 Q, per example, per waveform, per SNR). Such configuration reaches an overall accuracy of 0.94 for approximately 16 minutes training. Fig. 5 displays the learning curve of the proposed CNN architecture, monitoring both the accuracy and the categorical-entropy loss on the training and validation sets respectively. These figures show a good fit. Notice that we set the total number of epochs to 100, but using the early stopping method, the learning ends at 60 epochs since continued training of a good fit will likely lead to an overfit.

Fig. 6 presents different confusion matrices for different SNR values. An interesting behavior of the CNN for the lowest SNR case in our dataset, that is SNR$= -8$ dB, is the ability of the classifier to recognize GFDM with very high accuracy. Our intuition behind this behavior, is that this particular waveform exhibits very rich statistical features due to its subsymbols concept and circular filtering (as it was demonstrated with cyclostationarity [27]) rendering its recognition more accurate even with very small number of multicarrier symbols and with low SNR values. The classification performance increases for high SNR values, and reaches a total accuracy of 0.99 at SNR 2 dB, for the chosen configuration.

Fig. 7 shows the per class accuracy of the investigated CNN model. GFDM classification is the highest

TABLE 4. Training time.

Configuration	Training time (mm:ss)	Accuracy
CNN		
$N_s = 64,\ m = 2500$	06:33	0.9179
$N_s = 64,\ m = 3500$	12:50	0.9260
$N_s = 128,\ m = 2500$	15:33	0.9357
$N_s = 128,\ m = 3500$	23:40	0.9568
SVM		
$N_s = 100 \times N,\ m = 500$	00:06	0.9317
$N_s = 50 \times N,\ m = 2000$	04:50	0.8306
$N_s = 10 \times N,\ m = 2000$	06:03	0.6263

followed by F-OFDM, UFMC, FBMC then OFDM. This leads to the conclusion that, indeed, the filtering adopted in the investigated waveforms results in distinctive statistical features, which are captured and used by the CNN model to correctly classify these new transmission schemes.

Finally Fig. 8 displays a comparison between the several configurations, using the per SNR accuracy. We notice that using longer symbols, or more examples both increase the overall performance, for low SNR values. It is clear that starting from 2 dB, all configurations perform equally, hence increasing the number of examples only increases the complexity and training time.

For the cyclostationary based routine, we consider different configurations, as our features extraction method fails to extract any other CF or lag different than zeros, with very small number of symbols especially for low SNR values. We start with 10 symbols, then 50, and finally use the entire database, that is 100 multicarrier symbols to extract the α and τ profile. To reduce the complexity of our vector estimation, we construct only five cyclic frequencies ($n_c = 5$) for each waveform. We then feed this hand crafted features vector to an SVM with a linear kernel. The routine achieves an overall accuracy of 0.63, 0.83 and 0.93 for the three configurations respectively, for roughly 6, 5 and less than 1 minute training time each. Table 4 summarizes the training time and accuracy of all the considered cases.

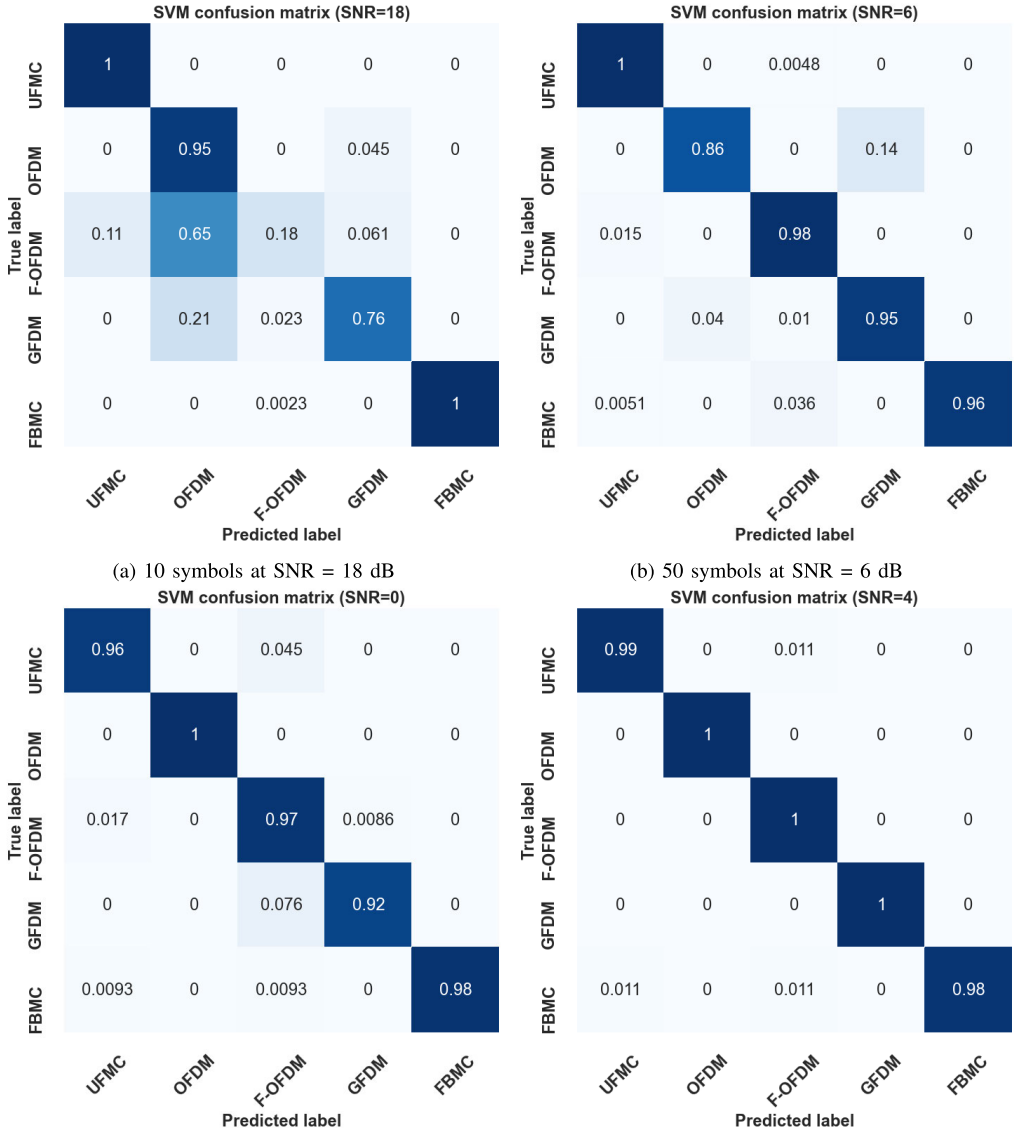

(a) 10 symbols at SNR = 18 dB

(b) 50 symbols at SNR = 6 dB

(c) 100 symbols at SNR =0 dB

(d) 100 symbols at SNR = 4 dB

FIGURE 9. Confusion matrices of the proposed CS + SVM, with different symbol lengths.

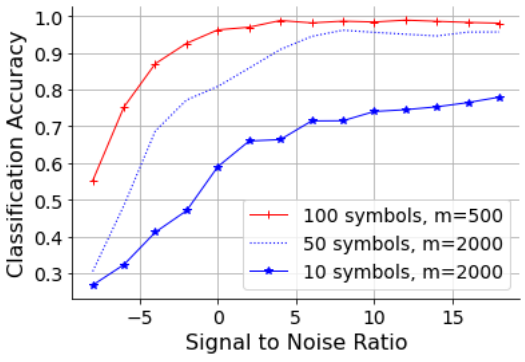

FIGURE 10. Accuracy comparison between 100, 50 and 10 symbols.

Fig. 9 shows the confusion matrices where the highest classification accuracy is achieved, that is at 18 dB for the 10-symbol case, 6 dB for the 50-symbol case, and 4 dB for the 100 symbols case. We can clearly see that using longer signals results in better estimation of the cyclic cumulant, since the error estimation of these features for noise reduces with the number of processed samples. These results are obtained using 2000 examples from the available dataset with again, 80% for training, and 20% for validation and testing; when using the 100 multicarrier symbols, good performance is achieved with only 500 examples. Compared to the DL-based approach the latter yields far better performance, as a total accuracy of 1 is achieved at lower SNR with shorter signals.

Finally, Fig. 10 represents the overall accuracy for the three considered configurations. From the figure, we notice that the cyclostationary based routine is stable with a higher number of multicarrier symbols and lower number of examples. In fact, the longer the processed signal is, the lower the

estimation error of the AWGN CC is, making the features vector more accurate.

V. CONCLUSION

In this paper, we have proposed and compared two different ASR techniques to classify multicarrier waveforms. The investigated transmission schemes are mainly filtered variants of the legacy OFDM, that offer higher spectral efficiency and are better suited for a wide variety of applications. They include, the per subband filtered family, namely UFMC and F-OFDM, and the per subcarrier filtered one, that is FBMC and GFDM. The use of different filtering techniques in these waveforms results in a rich pool of cyclic features, which we have taken advantage of to design a novel recognition routine based on their α and τ profile combined to an SVM classifier. Such technique follows the traditional expert knowledge based ASR. We then have compared it to the more advanced DNN based ASR, using a four-layer CNN that can autonomously extract discriminative features from the input signals then use them to classify the investigated waveforms. We have noticed an interesting behavior of the CNN with regard to the filtered multicarrier waveforms, the more complex is the filtering technique, the easiest it is to recognize it. The simulation results show that the CNN classifier outperforms the cyclostationarity based one, as it reaches an accuracy of 0.99 for SNR= 2 dB with only 2 multicarrier symbols, while the expert features one achieves an accuracy of 0.93 with 100 symbols. The main advantage of the SVM based routine is the lower number of training examples needed compared to the CNN, as the signals are preprocessed and reduced to a smaller features vector before being fed to the ML algorithm. In our future work, we will focus on extending the present DL-based ASR approach, using transfer learning to account for different channel propagation environments and enrich the pool of the investigated waveforms.

REFERENCES

[1] Y. Siriwardhana, C. De Alwis, G. Gur, M. Ylianttila, and M. Liyanage, "The fight against the COVID-19 pandemic with 5G technologies," *IEEE Eng. Manag. Rev.*, vol. 48, no. 3, pp. 72–84, Sep. 2020.

[2] N. Michailow, M. Matthe, I. S. Gaspar, A. N. Caldevilla, L. L. Mendes, A. Festag, and G. Fettweis, "Generalized frequency division multiplexing for 5th generation cellular networks," *IEEE Trans. Commun.*, vol. 62, no. 9, pp. 3045–3061, Sep. 2014.

[3] *Prototype Filter and Structure Optimization, D5.1*, document PHYDYAS_007, 2010.

[4] M. Bellanger, "FS-FBMC: An alternative scheme for filter bank based multicarrier transmission," in *Proc. 5th Int. Symp. Commun., Control Signal Process.*, May 2012, pp. 1–4.

[5] V. Vakilian, T. Wild, F. Schaich, S. ten Brink, and J.-F. Frigon, "Universal-filtered multi-carrier technique for wireless systems beyond LTE," in *Proc. IEEE Globecom Workshops (GC Wkshps)*, Dec. 2013, pp. 223–228.

[6] L. Zhang, A. Ijaz, P. Xiao, A. Quddus, and R. Tafazolli, "Subband filtered multi-carrier systems for multi-service wireless communications," *IEEE Trans. Wireless Commun.*, vol. 16, no. 3, pp. 1893–1907, Mar. 2017.

[7] J. Abdoli, M. Jia, and J. Ma, "Filtered OFDM: A new waveform for future wireless systems," in *Proc. IEEE 16th Int. Workshop Signal Process. Adv. Wireless Commun. (SPAWC)*, Jun. 2015, pp. 66–70.

[8] *F-OFDM Scheme and Filter Design*, Huawei, HiSilicon, dpocument 3GPP TSG RAN WG1 Meeting 85, 2016.

[9] A. Sahin, I. Guvenc, and H. Arslan, "A survey on multicarrier communications: Prototype filters, lattice structures, and implementation aspects," *IEEE Commun. Surveys Tuts.*, vol. 16, no. 3, pp. 1312–1338, 3rd Quart., 2014.

[10] R. Gerzaguet, D. Kténas, N. Cassiau, and J. Doré, "Comparative study of 5G waveform candidates for below 6 GHz air interface," in *Proc. ETSI Workshop Future Radio Technol.-Air Interface*, Sophia Antipolis, France, 2016, pp. 27–28.

[11] M. Van Eeckhaute, A. Bourdoux, P. De Doncker, and F. Horlin, "Performance of emerging multi-carrier waveforms for 5G asynchronous communications," *EURASIP J. Wireless Commun. Netw.*, vol. 2017, no. 1, p. 29, Dec. 2017.

[12] H. Shaiek, R. Zayani, Y. Medjahdi, and D. Roviras, "Analytical analysis of SER for beyond 5G post-OFDM waveforms in presence of high power amplifiers," *IEEE Access*, vol. 7, pp. 29441–29452, 2019.

[13] S. Buzzi, C. D'Andrea, D. Li, and S. Feng, "MIMO-UFMC transceiver schemes for millimeter-wave wireless communications," *IEEE Trans. Commun.*, vol. 67, no. 5, pp. 3323–3336, May 2019.

[14] I. Galdino Andrade, R. Zakaria, D. Le Ruyet, and M. L. R. de Campos, "Short-filter design for intrinsic interference reduction in QAM-FBMC modulation," *IEEE Commun. Lett.*, vol. 24, no. 7, pp. 1487–1491, Jul. 2020.

[15] W. Anwar, A. Krause, A. Kumar, N. Franchi, and G. P. Fettweis, "Performance analysis of various waveforms and coding schemes in V2X communication scenarios," in *Proc. IEEE Wireless Commun. Netw. Conf. (WCNC)*, May 2020, pp. 1–8.

[16] F. Meng, P. Chen, L. Wu, and X. Wang, "Automatic modulation classification: A deep learning enabled approach," *IEEE Trans. Veh. Technol.*, vol. 67, no. 11, pp. 10760–10772, Nov. 2018.

[17] X. Li, F. Dong, S. Zhang, and W. Guo, "A survey on deep learning techniques in wireless signal recognition," *Wireless Commun. Mobile Comput.*, vol. 2019, pp. 1–12, Feb. 2019.

[18] A. Punchihewa, Q. Zhang, O. A. Dobre, C. Spooner, S. Rajan, and R. Inkol, "On the cyclostationarity of OFDM and single carrier linearly digitally modulated signals in time dispersive channels: Theoretical developments and application," *IEEE Trans. Wireless Commun.*, vol. 9, no. 8, pp. 2588–2599, Aug. 2010.

[19] C. M. Spooner, A. N. Mody, J. Chuang, and J. Petersen, "Modulation recognition using second- and higher-order cyclostationarity," in *Proc. IEEE Int. Symp. Dyn. Spectr. Access Netw. (DySPAN)*, Mar. 2017, pp. 1–3.

[20] K. Hassan, I. Dayoub, W. Hamouda, and M. Berbineau, "Automatic modulation recognition using wavelet transform and neural network," in *Proc. 9th Int. Conf. Intell. Transp. Syst. Telecommun., (ITST)*, Oct. 2009, pp. 234–238.

[21] X. Zhou, Y. Wu, and B. Yang, "Signal classification method based on support vector machine and high-order cumulants," *Wireless Sensor Netw.*, vol. 2, no. 1, pp. 48–52, 2010.

[22] W. Liu, M. Kulin, T. Kazaz, A. Shahid, I. Moerman, and E. De Poorter, "Wireless technology recognition based on RSSI distribution at sub-nyquist sampling rate for constrained devices," *Sensors*, vol. 17, no. 9, p. 2081, Sep. 2017.

[23] T. J. O'Shea, J. Corgan, and T. C. Clancy, "Convolutional radio modulation recognition networks," in *Proc. Int. Conf. Eng. Appl. Neural Netw.* Cham, Switzerland: Springer, 2016, pp. 213–226.

[24] T. J. O'shea and N. West, "Radio machine learning dataset generation with gnu radio," in *Proc. GNU Radio Conf.*, 2016, vol. 1, no. 1, pp. 1–5.

[25] M. Kulin, T. Kazaz, I. Moerman, and E. De Poorter, "End-to-end learning from spectrum data: A deep learning approach for wireless signal identification in spectrum monitoring applications," *IEEE Access*, vol. 6, pp. 18484–18501, 2018.

[26] S. Duan, K. Chen, X. Yu, and M. Qian, "Automatic multicarrier waveform classification via PCA and convolutional neural networks," *IEEE Access*, vol. 6, pp. 51365–51373, 2018.

[27] K. Zerhouni, F. Elbahhar, R. Elassali, K. Elbaamrani, and N. Idboufker, "Influence of pulse shaping filters on cyclostationary features of 5G waveforms candidates," *Signal Process.*, vol. 159, pp. 204–215, Jun. 2019.

[28] C. W. Korevaar, A. B. J. Kokkeler, P.-T.-D. Boer, and G. J. M. Smit, "Spectrum efficient, localized, orthogonal waveforms: Closing the gap with the balian-low theorem," *IEEE Trans. Commun.*, vol. 64, no. 5, pp. 2155–2165, May 2016.

[29] C. Heil and A. M. Powell, "Gabor schauder bases and the balian-low theorem," *J. Math. Phys.*, vol. 47, no. 11, Nov. 2006, Art. no. 113506.

[30] K. Zerhouni, F. Elbahhar, R. Elassali, and K. Elbaamrani, "Blind parameters estimation for Universal Filtered Multicarrier: A cyclostationarity approach," in *Proc. Wireless Telecommun. Symp. (WTS)*, Apr. 2019, pp. 1–6.
[31] M. Matthe, D. Zhang, F. Schaich, T. Wild, R. Ahmed, and G. Fettweis, "A reduced complexity time-domain transmitter for UF-OFDM," in *Proc. IEEE 83rd Veh. Technol. Conf. (VTC Spring)*, May 2016, pp. 1–5.
[32] X. Zhang, M. Jia, L. Chen, J. Ma, and J. Qiu, "Filtered-OFDM–enabler for flexible waveform in the 5th generation cellular networks," in *Proc. IEEE Global Commun. Conf. (GLOBECOM)*, Dec. 2015, pp. 1–6.
[33] K. W. Martin, "Small side-lobe filter design for multitone data-communication applications," *IEEE Trans. Circuits Syst. II, Analog Digit. Signal Process.*, vol. 45, no. 8, pp. 1155–1161, 1998.
[34] M. G. Bellanger, "Specification and design of a prototype filter for filter bank based multicarrier transmission," in *Proc. IEEE Int. Conf. Acoust., Speech, Signal Process.*, vol. 4, May 2001, pp. 2417–2420.
[35] S. Mirabbasi and K. Martin, "Overlapped complex-modulated transmultiplexer filters with simplified design and superior stopbands," *IEEE Trans. Circuits Syst. II, Analog Digit. Signal Process.*, vol. 50, no. 8, pp. 456–469, Aug. 2003.
[36] F.-L. Luo and C. Zhang, *Signal Processing for 5G: Algorithms and Implementations*. Hoboken, NJ, USA: Wiley, 2016.
[37] O. Simeone, "A very brief introduction to machine learning with applications to communication systems," *IEEE Trans. Cognit. Commun. Netw.*, vol. 4, no. 4, pp. 648–664, Dec. 2018.
[38] O. A. Dobre, A. Abdi, Y. Bar-Ness, and W. Su, "Cyclostationarity-based modulation classification of linear digital modulations in flat fading channels," *Wireless Pers. Commun.*, vol. 54, no. 4, pp. 699–717, Sep. 2010.
[39] X. Liu, D. Yang, and A. E. Gamal, "Deep neural network architectures for modulation classification," in *Proc. 51st Asilomar Conf. Signals, Syst., Comput.*, Oct. 2017, pp. 915–919.
[40] T. O'Shea and J. Hoydis, "An introduction to deep learning for the physical layer," *IEEE Trans. Cognit. Commun. Netw.*, vol. 3, no. 4, pp. 563–575, Dec. 2017.
[41] M. Awad and R. Khanna, "Support vector machines for classification," in *Efficient Learning Machines*. Berkeley, CA, USA: Apress, 2015, pp. 39–66.
[42] A. Napolitano, "Cyclostationarity: New trends and applications," *Signal Process.*, vol. 120, pp. 385–408, Mar. 2016.
[43] W. A. Gardner, A. Napolitano, and L. Paura, "Cyclostationarity: Half a century of research," *Signal Process.*, vol. 86, no. 4, pp. 639–697, Apr. 2006.
[44] K. Zerhouni, R. Elassali, F. Elbahhar, K. Elbaamrani, and N. Idboufker, "On the cyclostationarity of universal filtered multi-carrier UFMC," *AEU-Int. J. Electron. Commun.*, vol. 89, pp. 174–180, May 2018.
[45] K. Zerhouni, "Contributions to radio environmental awareness of cognitive radio in 5G systems," Ph.D. dissertation, Elect. Telecommun. Eng., Cadi Ayyad Univ., Marrakesh, Morocco, 2018.
[46] N. A. El-Alfi, H. M. Abdel-Atty, and M. A. Mohamed, "Cyclostationary detection of 5G GFDM waveform using time smoothing algorithms in cognitive radio transmission," in *Proc. IEEE 17th Int. Conf. Ubiquitous Wireless Broadband (ICUWB)*, Sep. 2017, pp. 1–6.
[47] A. V. Dandawate and G. B. Giannakis, "Statistical tests for presence of cyclostationarity," *IEEE Trans. Signal Process.*, vol. 42, no. 9, pp. 2355–2369, 1994.
[48] A. Napolitano, "Cyclic statistic estimators with uncertain cycle frequencies," *IEEE Trans. Inf. Theory*, vol. 63, no. 1, pp. 649–675, Jan. 2017.
[49] (2020). *Lecture Notes on Convolutional Neural Networks for Visual Recognition*. Spring. [Online]. Available: http://cs231n.stanford.edu
[50] J. Brownlee, *Deep Learning With Python: Develop Deep Learning Models on Theano and TensorFlow using Keras* (Machine Learning Mastery). Melbourne, VIC, Australia, 2020.
[51] I. Goodfellow, Y. Bengio, and A. Courville, *Deep Learning*. Cambridge, MA, USA: MIT Press, 2016. [Online]. Available: http://www.deeplearningbook.org
[52] D. Kingma and J. Ba, "Adam: A method for stochastic optimization," in *Proc. Int. Conf. Learn. Represent.*, 2014.
[53] *User Equipment (UE) Radio Transmission and Reception*, document 3GPP, TS 36.101, 2016.
[54] *5G; NR; User Equipment (UE) Radio Transmission and Reception; Part 1: Range 1 Standalone*, document 3GPP, TS 38.101–1 version 15.2.0 Release 15, 2018.

KAWTAR ZERHOUNI received the M.S. degree in telecommunication and networking from the National School of Applied Sciences, Marrakesh, and the Ph.D. degree in telecommunication, electrical, and networking engineering from Cadi Ayyad University, in 2018. She is currently a Postdoctoral Researcher with the School of Computer Science, Mohammed VI Polytechnic University (UM6P), Morocco. Before joining UM6P, she was a Research Engineer with LEOST, IFSTTAR, France, where she actively participated in several European projects focusing on v2x technology. Her research interests include multicarrier waveforms, signal detection, cognitive radio, and machine learning.

EL MEHDI AMHOUD (Member, IEEE) received the Ph.D. degree in computer and communication sciences from Télécom ParisTech, France. He is currently an Assistant Professor with Mohammed VI Polytechnic University, Morocco. Prior to his current position, he was a Postdoctoral Research Fellow with the King Abdullah University of Science and Technology, Saudi Arabia. He holds several U.S. patents. His research interests include modeling and analyzing the performance of new generations of communication networks and the Internet of Things. He received two awards of excellence for his outstanding Ph.D. thesis from the Mines-Télécom Institute and the Marie Skłodowska-Curie Research Grant from the European Commission.

MARWA CHAFII (Member, IEEE) received the master's degree in the field of advanced wireless communication systems (SAR) and the Ph.D. degree in electrical engineering from CentraleSupélec, France, in 2013 and 2016, respectively. From 2014 to 2016, she has been a Visiting Researcher with the Poznan University of Technology, Poland; the University of York, U.K.; Yokohama National University, Japan; and the University of Oxford, U.K. In February 2018, she joined the Vodafone Chair Mobile Communications Systems, Technical University of Dresden, Germany, as a Research Group Leader. Since September 2018, she has been the Research Projects Lead with the Women in AI and an Associate Professor with ENSEA, France, where she is currently the Chair of excellence on artificial intelligence with the CY Initiative. Her research interests include machine learning for wireless communications, advanced waveform design, indoor localization, and channel estimation. She received the Prize of the Best Ph.D. in France in the fields of signal, image, and vision, and has been nominated in the Top Ten Rising Stars in Computer Networking and Communications by the N2Women, in 2020. Since 2019, she has been serving as an Associate Editor for IEEE COMMUNICATIONS LETTERS, where she received the Best Editor Award, in 2020. She is also the Vice-Chair of the IEEE ComSoc Emerging Technology Initiative on Machine Learning for Communications and managing the Gender Committee of the AI4EU Community.